The Canadian Mineralogist
Vol. 53, pp. 13-30 (2015)
DOI: 10.3749/canmin.1400079

HOGARTHITE, $(Na,K)_2CaTi_2Si_{10}O_{26}\cdot 8H_2O$, A NEW MEMBER OF THE LEMOYNITE GROUP FROM MONT SAINT-HILAIRE, QUEBEC: CHARACTERIZATION, CRYSTAL-STRUCTURE DETERMINATION, AND ORIGIN

ANDREW M. MCDONALD[§]

Department of Earth Sciences, Laurentian University, 935 Ramsey Lake Road, Sudbury, Ontario P3E 2C6, Canada

PETER TARASSOFF

Redpath Museum, McGill University, 859 Rue Sherbrooke O, Montréal, Quebec H3A 0C4, Canada

GEORGE Y. CHAO

2031 Delmar Drive, Ottawa, Ontario K1H 5P6, Canada

ABSTRACT

Hogarthite, $(Na,K)_2CaTi_2Si_{10}O_{26}\cdot 8H_2O$, a new mineral of the lemoynite group, was discovered in vugs within metasomatically altered marble xenoliths in the Poudrette quarry, Mont Saint-Hilaire, La-Vallée-du-Richelieu RCM, Montérégie, Quebec, Canada. Crystals are bladed to blocky, average 0.05 × 0.15 × 2 mm in size, and range in color from tan to white to colorless. The mineral develops in dense, radiating crystal aggregates up to 0.5 × 3 mm in size, and is associated with calcite (several generations), quartz, haineaultite, labuntsovite-Mn, lemoynite, chabazite, and gmelinite-Na. Crystals are elongate along [100], flattened on {010} and are bounded by the forms pinacoid {010} (dominant), pinacoid {100} (minor), and pinacoid {001} (minor). The mineral has a white streak, is non-fluorescent under short-, medium-, and long-wave ultraviolet radiation, is translucent, and has a satiny to silky to subvitreous luster. It has a brittle fracture, a perfect {010} cleavage, a hackly to splintery fracture, an estimated hardness of 4, and D_{calc} = 2.40(1) g/cm^3. Hogarthite is biaxial (+) with α 1.567(1), β 1.591 (1), and γ 1.618(1) with $2V_{meas}$ = 87(1)º and $2V_{calc}$ = 88(1)º. The optical orientation is $X = b$, $Y \wedge c$ = 15º (measured in the obtuse angle β), $Z = a$. A total of 21 analyses, obtained from seven crystals, gave an average (range) of (wt.%): Na_2O 2.37 (1.69–2.92), K_2O 2.88 (2.61–3.17), CaO 6.00 (5.40–6.31), TiO_2 14.44 (13.70–15.83), ZrO_2 1.11 (0.48–1.73), Nb_2O_5 0.78 (0.42–1.24), SiO_2 59.27 (57.32–60.64), H_2O 14.10 (calc.), total 100.95. The empirical formula (based on 34 anions) is $(Na_{0.78}K_{0.62}\square_{0.51}Ca_{0.09})_{\Sigma 2.00}Ca(Ti_{1.85}Zr_{0.09}Nb_{0.06})_{\Sigma 2.00}Si_{10.09}O_{26}\cdot 8H_2O$, and the simplified formula is $(Na,K)_2CaTi_2Si_{10}O_{26}\cdot 8H_2O$. The presence of (OH) and H_2O were confirmed *via* refinement of the crystal-structure and data from combined FTIR and Raman spectroscopies. The mineral crystallizes in space group $C2/m$ with a 10.1839(5), b 15.8244(6), c 9.1327(7) Å, β 104.463(2)º, V 1425.1(1) Å^3, and Z = 2. The strongest six lines on the X-ray powder diffraction pattern [d in Å (I) (*hkl*)] are: 8.835 (85) (001), 7.913 (100) (020), 6.849 (70) ($\bar{1}11$), 4.336 (45) ($\bar{1}31$, $\bar{1}12$), 3.514 (80) (221), 3.426 (55) ($\bar{2}22$, $\bar{1}32$). The crystal structure, refined to R = 0.049 for 1335 reflections ($F_o > 4\sigma F_o$), consists of a silicate component, composed of interconnected, non-planar 10-membered rings, arranged into thick slabs and stacked along [001]. These are interleaved with layers of independent TiO_6 octahedra, producing a framework of composition $[TiSi_5O_{13}]^{2-}$. Numerous channels within the framework, notably the continuous ones developed by 10-membered silicate rings, are occupied by Na, Ca, and H_2O groups. Hogarthite is considered to be a product of late-stage alkaline fluid enriched in SiO_2 and TiO_2, and forming under conditions of low P at T < 200 ºC, possibly through crystallization of a gel.

Keywords: Hogarthite, new mineral, titanosilicate, crystal structure, lemoynite group, crystallization conditions, Mont Saint-Hilaire, Quebec, Canada.

INTRODUCTION

Agpaitic (Na+K/Al > 1) geological environments are geochemically characterized by low SiO_2 contents along with pronounced enrichments in high-field-strength elements (*HFSE*; Ti, Zr, Nb). These two features are significant, as they can lead to the development of an abundance of unusual, silica-undersaturated

§ *Corresponding author e-mail address*: amcdonald@laurentian.ca

minerals in which the HFSE effectively proxy for Si. These can range from sorosilicate-like (*e.g.*, laurentianite; Haring *et al.* 2010), to inosilicate-like (*e.g.*, neptunite; Canillo *et al.* 1966), to simple and complex layered-like silicates (*e.g.*, astrophyllite-group minerals; Piilonen *et al.* 2003), to those based on frameworks (*e.g.*, haineaultite; McDonald & Chao 2004). Here we report on the new alkali titanosilicate hydrate mineral, hogarthite, a HFSE-dominant mesoporous silicate whose crystal-chemical features are highly reminiscent of zeolites and zeolitic-like minerals found in more SiO_2-rich environments. Its discovery is noteworthy, as it increases the number of known minerals related to lemoynite ($Na_4Zr_2Si_{10}O_{26}{\cdot}9H_2O$; Perrault *et al.* 1969) and serves to both broaden our crystal-chemical knowledge of the HFSE-dominant silicate minerals and the evolution of agpaitic rocks.

The mineral is named for Dr. Donald D. Hogarth (1929-), Professor Emeritus in the Department of Earth Sciences at the University of Ottawa, in recognition of his contributions to the mineralogy and geology of the Grenville Province in Quebec and Ontario, in particular carbonatites and related rocks from the Gatineau, Quebec area, and to the nomenclature of the pyrochlore group. Both the mineral and mineral name are approved by the Commission on New Minerals, Nomenclature and Classification of the IMA (IMA2009-043). Holotype material is housed in the collection of the Canadian Museum of Nature (Gatineau, Canada), catalogue number CMNMC 86086.

Occurrence

Hogarthite was first encountered by one of us (PT) on 22 June, 1986, on level 4 of the Poudrette quarry, Mont Saint-Hilaire, La-Vallée-du-Richelieu RCM, Montérégie (formerly Rouville County), Quebec, Canada. The mineral was discovered in unusual marble xenoliths consisting of two phases: (1) pale green to white, coarse-grained, granular calcite interspersed with small (<1 mm) stubby crystals of black clinoamphiboles (Na-rich), consistent with the typical marble encountered at the locality, and (2) a vuggy, dark-grey, dense marble composed of intergrown laths of pectolite, with lesser amounts of calcite, quartz, phlogopite (F-rich), and rare, pinkish laths that give an X-ray powder diffraction pattern similar to that of götzenite. The xenoliths were not observed *in situ,* but all were found in close proximity to one another, among blocks of rock set aside for secondary breakup. This suggests that they may have been part of a single, much larger, marble xenolith. Contacts between the dark and lighter-colored marble are irregular and diffuse (Fig. 1), possibly indicating dissolution of the latter. The dark marble also shows evidence of brecciation, especially near the contacts between the two marble types. This may indicate a precursor marble xenolith that had been entrapped during the late-stage development of an igneous breccia (Piilonen *et al.* 1998) and was subsequently metasomatized, an occurrence reminiscent of that observed for the eudialyte-group mineral johnsenite-(Ce) (Grice & Gault 2006).

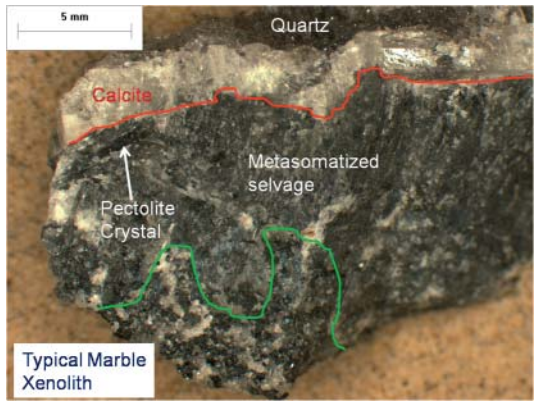

Fig. 1. Contacts between a typical marble xenolith and its metasomatized selvage (green) and between the selvage and vug (red). The image also shows a euhedral pectolite crystal in the metasomatized selvage.

Vugs in the dark marble are irregular in shape but are generally elongate (<2 cm in width and <5 cm in length) and appear to be concentrated near the contact with the pale marble. They are lined by coarse-grained, tabular to blocky, transparent, colorless, inclusion-free calcite that is, in part, overgrown by a secondary growth of calcite that is distinctly yellow in color. The calcite is overgrown by druses of small (<1 mm) colorless, euhedral, prismatic, quartz crystals. In some cases, sub- to euhedral crystals [cube {100}] of fluorite (<1 cm across) are included in the calcite. The contacts between the dark marble and the clear, colorless calcite lining the vugs are sharp and distinct. In rare cases, a tertiary generation of blocky, euhedral rhombohedrons of calcite (<1 mm) is observed to overgrow the quartz.

The majority of the vugs contain only calcite and quartz. In rare cases, some contain Ti-silicate minerals including the new species hogarthite, labuntsovite-Mn (based on qualitative SEM-EDS data), haineaultite [$(Na,Ca)_5Ca(Ti,Nb)_5Si_{12}O_{34}(OH,F)_8{\cdot}5H_2O$], and Zr-silicates including tumchaite and lemoynite, all of which post-date quartz. Hogarthite also develops in the dark marble, but spatially close to the vugs. The marble xenolith in which hogarthite was found is the same from which haineaultite (type-I; McDonald & Chao 2004) was also discovered. As this particular marble xenolith is heterogeneous, the associated mineralogy is summarized according to lithology and paragenesis in Table 1. The earliest lithology is the

TABLE 1. MINERAL ASSEMBLAGES IN THE DIFFERENT LITHOLOGIES OF THE HOGARTHITE OCCURRENCE

Species	Marble Xenolith	Metasomatic Selvage	Vugs
Sulfides			
Marcasite			X
Millerite			X
Molybdenite		X	
Pyrite			X
Sphalerite		X	
Halides			
Fluorite			X
Carbonates			
Bastnäsite-(Ce)			
Calcite	XXX	XX	
Calcite-I			XXX*
Calcite-II			XXX*
Calcite-III			X*
Phosphates			
Fluorapatite			X
Silicates			
Aegirine			X
Analcime			X
Chabazite			X*
Clinoamphibole (Na-rich)	XX	X	XX
Gmelinite-Na			X*
Götzenite-like		X	
Haineaultite			X*
Hogarthite			X*
Labuntsovite-Mn			X*
Lemoynite			X*
Microcline		XXX	X
Monteregianite-(Y)		XX	X
Pectolite	X	XX	XX
Phlogopite series (F-rich)			XX
Quartz			
Quartz-I			XXX*
Quartz-II			XX*
Steacyite			X
Tumchaite			X

The relative abundance of the minerals in each lithology is represented as follows: major = XXX; minor = XX; rare = X.
Minerals found in direct association with hogarthite are marked with an asterisk.

white marble, composed of calcite, with lesser amounts of a clinoamphibole and rare phlogopite. The second is the dark, metasomatically altered portion of the marble that is dominated by pectolite with lesser amounts of calcite and quartz, along with rare hogarthite and a götzenite-like mineral. The last is the vugs in which hogarthite was discovered. These are generally lined by calcite which in turn is overgrown by quartz. A relatively large number of additional minerals overgrowing quartz are also found in these vugs, some of which may or may not be directly associated with hogarthite (Table 1). Of note is the occurrence of HSFE-bearing minerals including the titanosilicates labuntsovite-Mn and haineaultite, and the zirconosilicates lemoynite and tumchaite, which collectively suggest the presence of late-stage, alkali- and alkaline-earth- and HFSE-rich fluids. It is noteworthy that, although three different alkali titanosilicate minerals are observed in the vug assemblage (*i.e.*, haineaultite, hogarthite, and labuntsovite-Mn), rarely are two of the three found on the same sample, and never are all three found together. This suggests that the fluids from which these minerals crystallized were geochemically similar, but distinct, an issue that is addressed later in this contribution.

Physical and Optical Properties

Hogarthite develops as dense, radiating crystal aggregates up to 0.5 × 3 mm in size (Fig. 2). Individual crystals are bladed to blocky, averaging 0.05 × 0.15 × 2 mm in size, and range in color from tan to white to colorless (Fig. 3a). Crystals may be color zoned along their length: tan closest to their nucleation site and fading to white or colorless in areas distal to this (Fig. 3b), whereas in others, the color zonation may be reversed. Results from qualitative SEM-EDS analyses do not show any noticeable difference in major- or minor-element chemistry between the color zones. Crystals are elongate along [100], flattened on {010}, and appear to be bounded by the forms pinacoid {010} (dominant), pinacoid {100} (minor), and pinacoid {001} (minor). The mineral has a white streak, shows no discernible

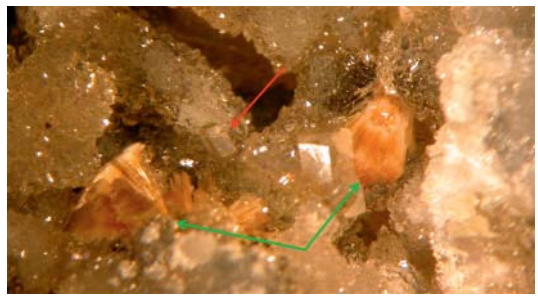

FIG. 2. Two radiating aggregates of tan-colored hogarthite (green arrows) with calcite-II (red arrow) and abundant crystals of drusy quartz (quartz-II). Field of view = 8 mm.

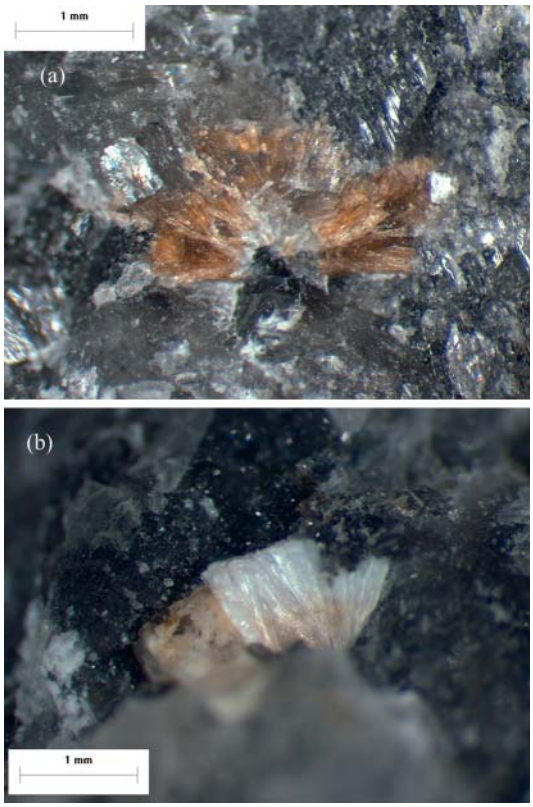

FIG. 3. (a) A tan radiating aggregate of hogarthite crystals from the metasomatized selvage and (b) a color-zoned aggregate showing crystals grading from tan (near nucleation point) to white.

fluorescence under short-, medium-, or long-wave ultraviolet radiation, is translucent, and has a satiny to silky to subvitreous luster. It has a brittle fracture, a perfect {010} cleavage, a hackly to splintery fracture, and an estimated hardness of 4. Density was not measured for the mineral; D_{calc} = 2.40(1) g/cm^3 was determined using the empirical chemical formula and the unit-cell parameters derived from the crystal-structure analysis. The mineral shows no effervescence or noticeable solubility in dilute (1:10) HCl.

Hogarthite is biaxial (+) with α 1.567(1), β 1.591(1), and γ 1.618(1) (λ = 590 nm) as measured with a spindle stage. The $2V_{meas}$ = 87(1)° with $2V_{calc}$ = 88(1)° and the orientation is $X = b$, $Y \wedge c = 15°$ (measured in the obtuse angle β), $Z = a$. Gladstone-Dale calculations gave a compatibility index of 0.029 (excellent) using the constants of Mandarino (1981).

CHEMICAL COMPOSITION

Chemical analysis of hogarthite was carried out with a Cameca SX-50 electron microprobe with an operating voltage of 15 kV, a beam current of 10 nA, and a beam diameter of 10 μm. For Na and Si, wavelength-dispersive data were collected, with data for all other elements being collected using the energy-dispersive mode. A total of seven elements were sought, and the following standards were employed: Na (*K*α, albite), K (*K*α, wadeite), Ca (*K*α, diopside), Ti (*L*α, syn. $MnTiO_3$), Zr (*L*α, wadeite), Nb (*L*α, syn. $FeNb_2O_4$), and Si (*K*α, wadeite), using count times of 100 s. Also sought, but not detected at concentrations greater than 1σ, were: Al, Mn, Fe, S, Hf, and F. A total of 21 analyses, obtained from seven crystals, gave an average (range) of (wt.%): Na_2O 2.37 (1.69–2.92), K_2O 2.88 (2.61–3.17), CaO 6.00 (5.40–6.31), TiO_2 14.44 (13.70–15.83), ZrO_2 1.11 (0.48–1.73), Nb_2O_5 0.78 (0.42–1.24), SiO_2 59.27 (57.32–60.64), H_2O 14.10 (calc.), total 100.95. The presence of (OH) and H_2O were confirmed *via* results of crystal-structure and Raman analyses (see below). The empirical formula (based on 34 anions) is: $(Na_{0.78}K_{0.62}\square_{0.51}Ca_{0.09})_{\Sigma 2.00}Ca(Ti_{1.85}Zr_{0.09}Nb_{0.06})_{\Sigma 2.00}Si_{10.09}O_{26}\cdot 8H_2O$, and the simplified formula is: $(Na,K)_2CaTi_2Si_{10}O_{26}\cdot 8H_2O$. The ideal formula, $Na_2CaTi_2Si_{10}O_{26}\cdot 8H_2O$, requires Na_2O 6.06, CaO 5.48, TiO_2 15.62, SiO_2 58.75, H_2O 14.09, total 100.00 wt.%. The empirical formula indicates a less-than-ideal sum for the site ascribed to *Na*, this being a weakly bound channel occupant in the crystal structure. We thus ascribe the low total for the *Na* site to the migration of alkalis under the electron beam. A vacancy is given in the empirical formula owing to the low sum for the alkali site, but the possibility of partial occupancy by hydronium ions cannot be discounted. The crystal structure of hogarthite contains a number of partially occupied H_2O sites (ranging from ¼ to ¾ of their ideal values) and the ideal number of H_2O given in the empirical formula has been calculated to reflect this.

INFRARED AND RAMAN ANALYSES

The infrared spectrum of hogarthite (Fig. 4a) was collected using a Bomem Michelson MB-120 Fourier-transform infrared spectrometer interfaced with a Spectra-Tech IR-Plan research microscope, equipped with a 0.25 mm (diameter) narrow-band, mercury-cadmium telluride detector. Samples were masked with a fixed 100 mm circular aperture prior to analysis. Single crystals of hogarthite were selected and individually mounted in a Spectra-Tech low-pressure diamond-anvil microsample cell and pressed into a thin film. The spectra were obtained over the range 600 to 4000 cm^{-1} (scanning resolution of ~4 cm^{-1}) from a total 200 co-added scans. Digital versions of the spectra are available from the Depository of Unpublished data on the Mineralogical Association of Canada (MAC) website [document hogarthite CM53_10.3749/canmin.1400079].

The Raman spectrum of hogarthite, covering a spectral range of 50 to 4000 cm^{-1} (scanning resolution of

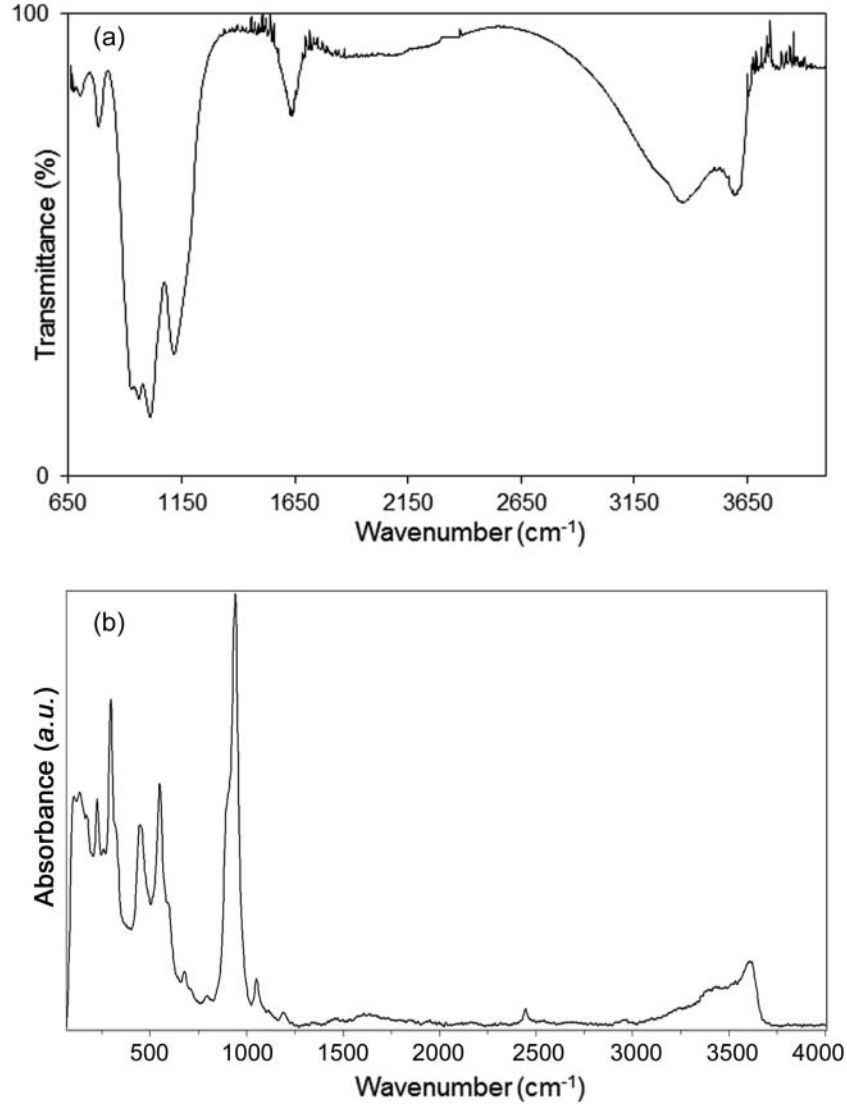

FIG. 4. (a) FTIR and (b) Raman spectra of hogarthite.

~2 cm^{-1}), was collected using a Horiba JobinYvon XPLORA confocal Raman system interfaced with an Olympus BX 41 microscope (Fig. 4b). Data were collected perpendicular to the {010} cleavage from a single crystal. The spectrum was obtained using three 20-second acquisition cycles, a 100×/0.75 objective lens, a grating of 1200 lines/mm, and a wavelength of $\lambda = 532$ nm. A digital version of the spectrum is available from the Depository of Unpublished data on the MAC website [document hogarthite CM53_10.3749/canmin.1400079].

Data pertaining to absorption strength, peak shape, position, and assignment of the bands in both the FTIR and Raman spectra are given in Tables 2a and 2b, respectively. Absorption bands were initially identified using data from Farmer (1974); specific assignments of those bands involving Ti–O–Si chains were made using data provided by Celestian *et al.* (2013) for synthetic sitinakite, $HNa_2KTi_4Si_2O_{14}·4H_2O$, whose Raman spectrum is very similar to that of hogarthite. In general, the two vibrational spectra for hogarthite are quite similar to one another, such that absorption bands in both spectra can be discussed in terms of four major groupings: (1) bands at >3000 cm^{-1}; (2) bands between 700 and 1200 cm^{-1}; (3) bands between 400 and 700 cm^{-1}; and (4) bands

TABLE 2A. INFRARED DATA FOR HOGARTHITE

Band (cm^{-1})	Peak breadth	Relative intensity	Designation
3612	relatively sharp	strong	O–H stretch
3372	relatively broad	strong	"
3246	broad	moderately strong	"
1645	relatively sharp	strong	H–O–H bend
1126	sharp	very strong	Si–O stretch
1016	sharp	very strong	"
968	sharp	very strong	"
935	sharp	very strong	"
788	sharp	moderately strong	Si–O bend
712	sharp	moderately strong	"
678	sharp	moderately strong	"

TABLE 2B. RAMAN DATA FOR HOGARTHITE

Band (cm^{-1})	Peak breadth	Relative intensity	Designation
3607	moderately broad	moderately weak	O–H stretch
3411	very broad	weak	"
3239	very broad	very weak	"
1608	very broad	weak	H–O–H bend
1190	broad	weak	Si–O stretch
1052	sharp	moderately weak	"
942	sharp	very strong	"
902	moderately sharp	strong	"
794	relatively broad	weak	Si–O bend
714	relatively broad	weak	"
679	moderately sharp	weak	"
548	sharp	strong	Ti–O stretch
448	sharp	strong	"
295	sharp	strong	Ti–O–Si,Ti–O–Ti stretch
258	sharp	very weak	"
225	sharp	moderately strong	"
173	relatively sharp	moderately weak	Lattice vibrations
135	relatively sharp	weak	"
105	relatively sharp	weak	"

<400 cm^{-1}. The first grouping is assigned to O–H stretching, and the presence of at least three peaks suggests the presence of at least three crystallographically distinct H_2O groups. There is also a band ~1600 cm^{-1} in both spectra that may be ascribed to H–O–H bending. Whereas this indicates H_2O is present in hogarthite (also confirmed by refinement of the crystal structure), the band is broad and relatively weak in both spectra, probably reflecting the strongly disordered nature of the H_2O groups in the mineral. The weakness of this absorption band in the Raman spectrum may also be related to the orientation of the grain analyzed, as Raman spectra can be sensitive to such effects. The second major grouping, centered near 1000 cm^{-1} and clearly dominating the overall spectrum, is assigned to Si–O stretches. Here, there appear to be three peaks in the FTIR spectrum, one of which (~960 cm^{-1}) may be resolved into a doublet. This would infer the presence of up to four crystallographically distinct SiO_4 groups, but results from analysis of the crystal structure indicate only three, so it is possible that the peak at ~960 cm^{-1} is not a true doublet. Interestingly, the Raman spectrum in this same region also suggests the presence of four bands, albeit at different energies, with the lowest energy band (~800 cm^{-1}) being extremely weak. It is also noteworthy that the spectrum of sitinakite also shows four bands in this region, despite the fact that results

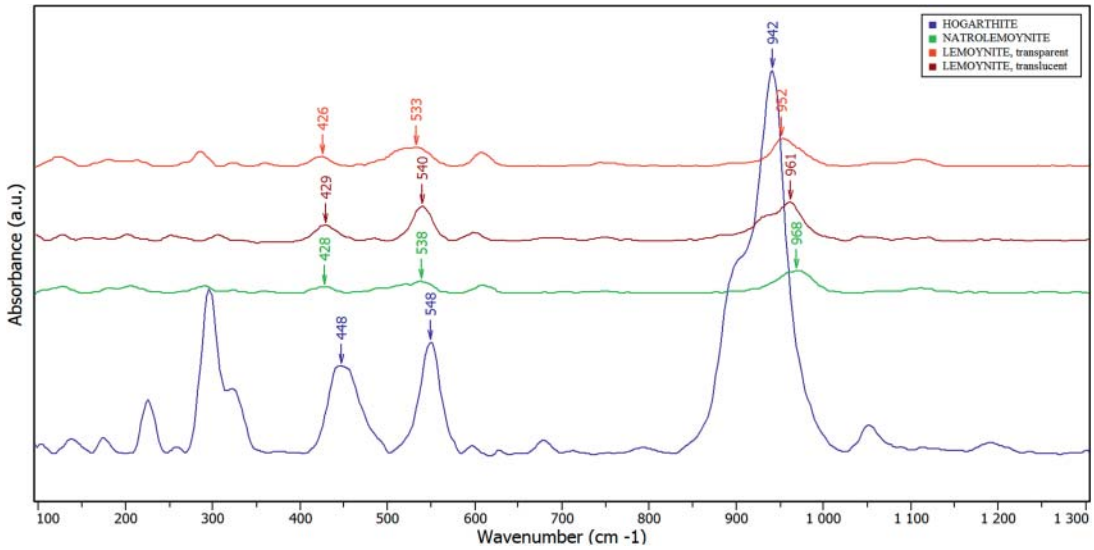

FIG. 5. A comparison of the Raman spectra for hogarthite, natrolemoynite, and lemoynite, showing absorption-band shift as a function of the type of HFSE present.

from the crystal-structure analysis (Sokolova *et al.* 1989) indicate the presence of only one crystallographically unique SiO_4 group. The third and fourth regions are relatively strong in the Raman spectrum, but much less so in the FTIR spectrum. Bands in the area 600–400 cm^{-1} are attributed primarily to Ti–O stretching but may also involve vibrations related to Ti–O–Si linkages that are present in the crystal structure. Bands in the region <400 cm^{-1} are primarily attributed to a combination of Ti–O–Si and Ti–O–Ti bending, with those at lowest energies being attributed to lattice vibrations.

The Raman spectrum of hogarthite is very similar to that of other members of the lemoynite group and a comparison of these is given in Figure 5. A detailed examination of the spectra reveals that three of the strong bands (~430, 540, and 950 cm^{-1}) show subtle, but systematic variations, for that of hogarthite (Ti-dominant) compared to other lemoynite-group minerals (Zr-dominant). The variations are considered significant, based on an instrumental resolution of 2 cm^{-1}, and the fact that the averages for the respective peak positions (Table 3) reflect multiple analyses collected from several crystals of each species. The Raman spectra of all the minerals possess two strong bands in the 400–600 cm^{-1} region that can be attributed to *M*–O stretching (*M* = Zr or Ti; Table 3). In hogarthite, these bands are shifted to higher energy (*i.e.*, >430 and >540 cm^{-1}) relative to the Zr-dominant group members (*i.e.*, <430 and <540 cm^{-1}), with data pertaining to this being given in Table 3. The differences here may be attributed to the smaller ionic radius of $^{[6]}Ti^{4+}$ (0.605 Å) *versus* $^{[6]}Zr^{4+}$ (0.72 Å; Shannon 1976), this resulting in stronger bonding in hogarthite (Ti-dominant) relative to lemoynite and natrolemoynite (Zr-dominant). At the same time, the very intense band near 950 cm^{-1} is shifted to lower energy in hogarthite relative to lemoynite and natrole-

TABLE 3. COMPARISON OF IMPORTANT RAMAN ABSORPTION BANDS [PEAK POSITION (ERROR)] IN LEMOYNITE-GROUP MINERALS

	n	~430 cm^{-1} band	~540 cm^{-1} band	~950 cm^{-1} band
Hogarthite	11	444 (4)	547 (4)	939 (3)
Lemoynite, translucent	7	427 (2)	538 (3)	964 (3)
Lemoynite, transparent	6	425 (2)	533 (3)	954 (5)
Natrolemoynite	4	425 (4)	539 (3)	966 (3)

moynite (>950 cm^{-1}). This particular band is attributed to Si–O stretching (Table 2b) and, given that the members of the lemoynite group possess crystal structures composed of a titanosilicate framework, the stronger Ti–O bonds in hogarthite likely lead to a minor weakening of the overall Si–O bonding relative to the Zr-dominant counterparts, and thus a relative reduction in the energies related to the Si–O absorption bands.

X-Ray Crystallography and Crystal-Structure Determination

X-ray powder diffraction data for hogarthite (Table 4) were collected using a 114.6 mm diameter Gandolfi camera, a 0.3 mm collimator, and Ni-filtered Cu*K*α radiation (λ = 1.5418 Å). Intensities were determined from a scanned image of the powder pattern using the program DIIS (Petrus *et al.* 2012) and normalized to the measured intensity of d = 7.912 Å (I = 100). To determine the contribution of an individual *hkl* plane to a reflection, the measured intensities were compared with a pattern calculated using results from the crystal-structure analysis and the program CRYSCON (Dowty 2002). Overall, there is a very good agreement between the measured and calculated powder patterns. The PXRD pattern of hogarthite resembles those of other lemoynite-group minerals (McDonald & Chao 2001), but the distribution of the six strongest lines is somewhat distinctive.

A brown crystal of hogarthite, measuring 20 × 30 × 120 μm and showing a sharp extinction under cross-polarized light, was selected for a single-crystal X-ray diffraction study. It was attached to a tapered glass fiber and mounted on a Bruker *P*4 diffractometer equipped with a Smart 1K CCD area detector (diameter of 9 cm, 512 × 512 pixels) and a fixed detector-to-crystal distance of 4.045 cm. Intensity data were collected to 60° 2θ using frame widths (ω) of 0.06° and exposure times of 100 s per frame. An empirical absorption correction was applied (SADABS; Sheldrick 2008a) and the data were corrected for Lorentz, polarization, and background effects. All reflection data were then merged using the program XPREP. Information relevant to the data collection and crystal-structure determination of hogarthite is given in Table 5.

The Oscail system (McArdle *et al.* 2004) which implements the SHELX-97 package of programs (Sheldrick 1997) was used for the solution and refinement of the crystal structure. Phasing of a set of normalized-structure factors gave a mean $|E^2-1|$ value of 0.885 (predicted values: 0.968 for centrosymmetric and 0.736 non-centrosymmetric); in light of the observed crystal morphology and the space-group symmetry exhibited by other members of the lemoynite group (McDonald & Chao 2001), hogarthite is

TABLE 4. POWDER X-RAY DIFFRACTION DATA FOR HOGARTHITE

*I*obs*	*I*calc**	*d*obs (Å)	*d*calc (Å)	*h*	*k*	*l*
85	**50**	**8.835**	**8.843**	**0**	**0**	**1**
3	3	8.348	8.369	1	1	0
100	**100**	**7.913**	**7.912**	**0**	**2**	**0**
70	**36**	**6.849**	**6.846**	**$\bar{1}$**	**1**	**1**
5	6	5.902	5.897	0	2	1
40	19	5.526	5.522	$\bar{1}$	1	1
10	8	4.861	4.853	$\bar{2}$	0	1
1	1	4.656	4.651	1	3	0
1	6	4.439	4.422	0	0	2
45	**23**	**4.336**	**4.332**	**$\bar{1}$**	**3**	**1**
	10		**4.304**	**$\bar{1}$**	**1**	**2**
10	10	4.189	4.185	2	2	0
10	7	3.913	3.911	2	0	1
10	9	3.865	3.860	0	2	2
1	1	3.788	3.797	$\bar{2}$	0	2
10	6	3.620	3.611	0	4	1
80	**50**	**3.514**	**3.506**	**2**	**2**	**1**
55	**18**	**3.426**	**3.423**	**$\bar{2}$**	**2**	**2**
	18		**3.412**	**$\bar{1}$**	**3**	**2**
3	2	3.225	3.218	3	1	0
5	5	3.094	3.086	2	4	0
20	12	3.036	3.031	$\bar{1}$	3	2
30	10	2.981	2.986	$\bar{1}$	1	3
	18		2.970	$\bar{3}$	1	$\bar{2}$
15	12	2.872	2.865	$\bar{2}$	0	$\bar{3}$
5	6	2.847	2.839	$\bar{3}$	3	1
50	18	2.792	2.788	1	5	1
	14		2.781	2	4	1
25	13	2.755	2.761	$\bar{2}$	2	2
5	7	2.702	2.694	$\bar{2}$	2	3
3	4	2.638	2.637	0	6	0
3	5	2.591	2.584	$\bar{1}$	5	2
10	7	2.550	2.545	$\bar{4}$	0	1
1	1	2.465	2.465	$\bar{4}$	0	0
1	1	2.429	2.426	$\bar{4}$	0	2
	1		2.423	$\bar{4}$	2	1
7	5	2.369	2.363	2	4	2
7	3	2.328	2.326	2	6	0
1	1	2.291	2.291	2	0	3
5	1	2.000	2.237	4	0	1
10	4	2.208	2.200	2	2	3
1	5	2.194	2.187	$\bar{2}$	6	1
1	1	2.171	2.167	$\bar{1}$	7	1
	1		2.166	$\bar{2}$	6	2
3	1	2.104	2.111	$\bar{1}$	7	1
	1		2.100	$\bar{4}$	2	3
1	1	2.063	2.068	$\bar{4}$	4	2
5	1	2.024	2.019	$\bar{5}$	1	1
	2		2.018	$\bar{1}$	7	2
15	7	1.986	1.982	2	4	3
10	4	1.958	1.957	5	1	0
	2		1.956	4	0	2
5	4	1.904	1.898	$\bar{4}$	0	4

TABLE 4. (CONTINUED)

*I*obs*	*I*calc**	*d*obs (Å)	*d*calc (Å)	*h*	*k*	*l*
3	1	1.850	1.847	5	3	0
	1		1.846	4	2	4
5	3	1.838	1.836	2	8	0
3	1	1.820	1.818	2	0	5
1	2	1.806	1.801	4	6	0
1	1	1.774	1.769	0	0	5
1	2	1.758	1.753	4	4	2
3	2	1.730	1.722	1	3	5
3	2	1.715	1.712	5	5	1
5	2	1.696	1.694	0	6	4
	2		1.694	6	0	1
5	4	1.670	1.669	3	5	3
7	2	1.648	1.645	5	1	2
7	3	1.640	1.636	3	7	2
1	1	1.617	1.616	5	3	4
1	1	1.610	1.609	6	2	0
5	3	1.588	1.585	6	2	3
1	2	1.565	1.562	4	8	1
3	4	1.536	1.532	3	5	5
3	2	1.526	1.522	1	9	3
10	1	1.520	1.520	3	9	2
	1		1.519	6	2	1
1	2	1.4982	1.4972	6	4	3
7	1	1.4711	1.4711	5	1	3
1	2	1.4510	1.4483	4	2	4
1	2	1.4444	1.4415	6	4	1
1	1	1.4350	1.4324	4	0	6
3	1	1.4238	1.4235	1	11	0
5	1	1.4138	1.4134	1	11	1
5	1	1.3980	1.3975	1	11	1
1	1	1.3846	1.3841	3	7	5
1	1	1.3755	1.3789	6	6	3
1	1	1.3537	1.3519	2	8	4
1	1	1.3381	1.3388	5	5	3
7	1	1.3211	1.3191	7	5	2
1	1	1.3064	1.3061	2	2	6
7	1	1.2900	1.2902	1	1	7
7	2	1.2835	1.2823	6	8	2
1	1	1.2766	1.2754	4	2	5
1	1	1.2668	1.2651	1	9	5
1	1	1.2588	1.2592	4	0	7
1	1	1.2547	1.2542	8	0	3
1	1	1.2431	1.2423	7	5	4
1	1	1.2329	1.2326	8	0	0
3	1	1.2214	1.2212	5	9	4
5	1	1.2138	1.2132	8	0	4
1	1	1.2055	1.2054	2	8	6
1	1	1.1839	1.1835	2	6	6
1	1	1.1554	1.1532	6	10	2
1	1	1.1406	1.1404	8	6	1
3	1	1.1064	1.1054	0	0	8
1	1	1.0846	1.0852	3	11	4
3	1	1.0712	1.0711	7	9	4
1	1	1.0678	1.0674	6	2	5

considered to be centrosymmetric. From a list of possible space-group choices, *C*2/*m* was selected. The crystal structure was solved by direct methods using scattering curves taken from Cromer & Mann (1968) and Cromer & Liberman (1970), respectively. An *E*-map was produced using calculated phase-normalized factors from which the *Si*, *Ti*, *Na*, *Ca*, and most of the *O* sites were located. Subsequent difference Fourier maps were used to locate the remaining *O* sites. Refinement of this model indicated several things: (1) the site-occupancy factor (*sof*) for the site assigned to *Ca* refined to 0.24, ~½ of the ideal value, so the *sof* was fixed at ½; (2) the site assigned to *Na* was fully occupied, *i.e.*, no evidence for the presence of K, Ca, or vacancies and attempts to refine these along with Na failed; (3) the *sof* for three of the sites assigned to H_2O, namely OW8, OW9, and OW10, refined to ~½ of the ideal value and were each subsequently fixed at 0.5; OW8 and OW9 refined to positions such that the two are separated by 1.33(1) Å, implying that the two sites cannot be occupied simultaneously. As such, the *sof* for two of the sites assigned to H_2O, namely OW11 and OW12, refined to values of ~¾ and ¼, respectively, and were subsequently fixed at these values. The final structure of hogarthite refined to R = 4.89% and wR_2 = 12.40%, with anisotropic displacement factors for all atoms. The final difference map calculated at this stage indicated a positive maximum of ~1 e^-/Å^3.

Table 6 contains the final positional and equivalent isotropic and anisotropic displacement parameters, and Table 7 contains selected interatomic distances and Table 8 gives bond-valence sums. Observed and calculated structure factors have been submitted to the Directory of Unpublished Data, CISTI, National Research Council of Canada, Ottawa, Ontario, Canada K1A 0S2.

Crystal Structure

The crystal structure of hogarthite can be described as a titanosilicate framework with channels wherein large cations and water molecules are housed. There are three crystallographically distinct SiO_4 tetrahedra present: two of these, *Si*(1)O_4 and *Si*(2)O_4, are joined into four-membered chains elongate along [010]. These form a discontinuous layer in the *ab* plane, with two symmetrically related layers being linked *via* *Si*(3)O_4 tetrahedra along [001]. The linkage

*Intensities visually estimated. **Calculated from the refined crystal structure. The six strongest lines are indicated in bold.
Pattern also includes a line at d = 3.351 Å that is not indexable on the cell proposed for hogarthite. Given this value, the X-ray diffraction data published for quartz (PDF card 46-1045) and the association of hogarthite with quartz, this line is attributed to the presence of a trace amount of quartz in the sample analyzed.

TABLE 5. MISCELLANEOUS CRYSTALLOGRAPHIC AND CRYSTAL-STRUCTURE REFINEMENT DATA FOR HOGARTHITE

Space Group	*C* 2/*m*	2θ Limit (°)	60
a (Å)	10.1839(5)*	Measured Reflections	6739
b	15.8244(6)*	Unique Reflections	2144
c	9.1327(7)*	Observed Reflections [$F_o > 4\sigma(F_o)$]	1335
β (°)	104.463(2)*	R_{merge}	0.076
V (Å^3)	1425.1(1)	GoOF	0.967
Z	2	Final *R* for all Observed Reflections	0.049
μ(Mo*K*α)	1.327 mm^{-1}	Final wR_2 for all Observed Reflections	0.113
Ideal unit cell contents	$2[(Na,K)_2CaTi_2Si_{10}O_{26}\cdot 8H_2O]$		

*values refined from four-circle diffractometer data

produces 10-membered silicate rings (cavity ~8.3 × 8.7 Å) when viewed along [102] (Fig. 6a), or one of two six-membered rings (cavities ranging from ~4.2 × 5.4 to ~5.0 × 6.2 Å) when viewed along [010] (Fig. 6b); these are significant as they create channels within which large cations and water molecules are accommodated. Importantly, bonding between the SiO_4 tetrahedra leads to development of thick (~6.5 Å) silicate layers ('slabs'), with successive silicate slabs being stacked along [001]; these are in turn joined by interleaving layers of TiO_6 octahedra, completing a titanosilicate framework of composition $[TiSi_5O_{13}]^{2-}$ (Fig. 7). It may be noteworthy that the TiO_6 octahedra are isolated from one another, *i.e.*, no direct Ti–O–Ti linkages are present, an atypical configuration relative to other titanosilicates (*e.g.*, labuntsovite-group minerals). As noted, the resulting framework results in a complex array of continuous and discontinuous channel types, the largest and most important of which are the continuous channels along [102] created by the 10-membered silicate rings, which easily accommodate the extra framework components of the mineral (Fig. 8).

The silicate component of the crystal structure of hogarthite may also be regarded as a two-dimensional loop-branched silicate in which the SiO_4 tetrahedra are joined into chains of periodicity four (oriented along [110]), with linkages between chains producing 10-membered loops or rings (Fig. 9; Liebau 1985). Alternatively, it may simplify things to consider the silicate component as a series of interconnected, nonplanar, 10-membered rings. The crystal structure is completed through the presence of Na and Ca as the 'soft' cations and Ti as the 'hard' cation, following the classification scheme of Liebau (1985).

Topology and Crystal-Structure Relationships

All members of the lemoynite group (Table 9) have framework crystal structures characterized by thick, double-silicate layers ('slabs') linked by layers of isolated MO_6 octahedra, with alkalis, alkaline-earths, and water molecules occupying channels. Minerals whose crystal structures are based on frameworks of tetrahedra and octahedra with large channels like this are referred to as Microporous Heterosilicate Minerals (MHM; Chukanov & Pekov 2005). These have crystal structures similar to those of zeolites but differ in that the latter have frameworks based solely on cation tetrahedra (typically Si, Al), whereas MHM have frameworks based on a combination of both cation tetrahedra (typically Si; *T*) and cation polyhedra of coordination >[4] (typically [6], with the cation being a HFSE, *i.e.*, Ti, Zr, Nb, and Y; *M*). The *T*:*M* ratios for MHM typically range from >2 to <8, among which two broad categories exist: (1) those with $3 < T{:}M < 8$, whose crystal structures are based on *T* cations forming chains (*e.g.*, gaidonnayite), bands (*e.g.*, elpidite), or layers (*e.g.*, penkvilksite), that are in turn linked by isolated MO_6 octahedra to complete a 3*D* framework, and (2) those with $1.6 < T{:}M < 3.6$, where the degree to which the *T* components are polymerized is reduced and whose crystal structures are based on Si_nO_{3n} rings (n = 3, 4, 6, 8) or Si_2O_7 groups connected by MO_6 octahedra that are isolated (*e.g.*, catapleiite), or in groups (*e.g.*, eudialyte) or chains (*e.g.*, labuntsovite-Mn). It is interesting to note that the crystal structure of hogarthite has features in common with both ring and layered silicates; in this sense, the crystal structure of hogarthite may be considered to be intermediate between titanosilicate minerals with structures based on true ring-silicate configurations (*e.g.*, benitoite) and those with layered-silicate configurations (*e.g.*, astrophyllite-group minerals). In light of the above classification scheme, and given the occurrence of three titanosilicate minerals in the vugs along with hogarthite (Table 1), a paragenetic sequence based on crystal-chemical relationships can be developed. First, labuntsovite-Mn with the lowest *T*:*M* ratio (2), has a crystal structure dominated by complexes of TiO_6 octahedra linked by

TABLE 6. FINAL POSITIONAL AND DISPLACEMENT PARAMETERS (Å^2) FOR HOGARTHITE

Atom	*x*	*y*	*z*	SOF	U_{11}	U_{22}	U_{33}	U_{23}	U_{13}	U_{12}	Ueq
Ca	1/2	0.3936(2)	0	0.5	0.021(1)	0.021(1)	0.027(2)	0	0.012(1)	0	0.0219(6)
Na	0.0954(4)	1/2	–0.1168(6)	1	0.045(2)	0.040(2)	0.155(5)	0	0.008(3)	0	0.083(2)
Ti	1/4	1/4	0	1	0.0079(4)	0.0130(5)	0.0077(5)	–0.0032(4)	0.0012(4)	0.0014(4)	0.0097(2)
Si1	–0.0496(1)	0.29075(7)	–0.2220(1)	1	0.0102(5)	0.0132(5)	0.0101(6)	0.0001(4)	0.0037(4)	0.0013(4)	0.0110(2)
Si2	0.2848(1)	0.40010(7)	0.2499(1)	1	0.0113(2)	0.0144(2)	0.0119(2)	0	0.0019(3)	0	0.0125(2)
Si3	1/2	0.3072(1)	1/2	1	0.0127(7)	0.0139(8)	0.0086(8)	0	0.0005(6)	0	0.0121(3)
O1	–0.1292(3)	0.3818(2)	–0.2551(3)	1	0.012(1)	0.016(1)	0.018(2)	0.004(1)	0.006(1)	0.003(1)	0.0150(6)
O2	0.3800(3)	0.3662(2)	0.4067(4)	1	0.023(2)	0.029(2)	0.016(2)	0.004(1)	–0.001(1)	0.008(1)	0.0238(7)
O3	–0.0593(3)	0.2506(2)	–0.3878(3)	1	0.024(1)	0.026(2)	0.014(2)	–0.002(1)	0.007(1)	0.006(1)	0.0210(7)
O4	0.3055(4)	1/2	0.2414(3)	1	0.017(2)	0.011(2)	0.032(3)	0	0.010(2)	0	0.019(1)
O5	–0.1316(3)	0.2304(2)	–0.1346(3)	1	0.014(1)	0.015(2)	0.018(2)	0.003(1)	0.010(2)	0.001(1)	0.0148(6)
O6	0.1043(2)	0.3117(2)	–0.1352(3)	1	0.010(1)	0.020(2)	0.021(2)	0.005(1)	0.002(1)	0.000(1)	0.0174(6)
O7	0.3188(3)	0.3556(2)	0.1057(3)	1	0.016(1)	0.017(2)	0.016(2)	–0.006(1)	0.007(1)	–0.005(1)	0.0158(6)
OW8	0.2655(10)	0.4163(6)	–0.159(1)	0.25	0.016(5)	0.004(5)	0.014(6)	–0.003(4)	0.009(5)	–0.005(4)	0.010(2)
OW9	0.352(1)	0.4401(8)	–0.240(1)	0.5	0.134(10)	0.087(9)	0.066(8)	–0.003(7)	–0.004(8)	0.042(8)	0.101(4)
OW10	1/2	0.4516(8)	0	0.5	0.076(8)	0.030(6)	0.059(8)	0	0.053(7)	0	0.049(3)
OW11	0.195(1)	0.4058(6)	–0.375(1)	0.75	0.34(2)	0.082(6)	0.157(10)	–0.013(7)	0.19(1)	–0.013(8)	0.168(5)
OW12	0.001(3)	1/2	–0.392(6)	0.5	0.13(2)	0.16(2)	0.66(10)	0	0.22(3)	0	0.30(3)

TABLE 7. SELECTED INTERATOMIC DISTANCES (Å) IN HOGARTHITE

Na–	Dist.	*vu*	Ca–	Dist.	*vu*	Ti–	Dist.	*vu*
OW8 ×2	2.29(1)	0.16	O7 ×2	2.364(3)	0.16	O6 ×2	1.940(3)	0.16
OW12	2.46(5)	0.16	OW9 ×2	2.44(1)	0.16	O5 ×2	1.950(3)	0.16
O1 ×2	2.981(4)	0.11	OW10	2.45(1)	0.11	O7 ×2	1.969(3)	0.11
O6 ×2	2.987(3)	0.11	OW8 ×2	2.49(1)	0.11	Mean/sum	1.953	0.92
Mean/sum	2.710	0.92	O5 ×2	2.517(4)	0.10			
			Mean/sum	2.451	0.92			
Si1–	Dist.	*vu*	Si2–	Dist.	*vu*	Si3–	Dist.	*vu*
O6	1.605(3)	0.46	O4	1.599(1)	1.26	O3 ×2	1.600(3)	1.24
O5	1.606(3)	0.46	O7	1.606(3)	1.22	O2 ×2	1.603(3)	1.22
O3	1.623(3)	0.45	O2	1.608(3)	1.22	Mean/sum	1.602	4.88
O1	1.643(3)	0.45	O1	1.623(3)	1.18			
Mean/sum	1.619	3.06	Mean/sum	1.609	4.88			

$(Si_4O_{12})^{-12}$ rings; next, haineaultite, with a slightly higher *T*:*M* ratio (2.4), has a crystal structure based on chains of TiO_6 octahedra linked by bands of SiO_4 tetrahedra [xonotlite-type, $(Si_6O_{17})^{-10}$], and finally, hogarthite, with the highest *T*:*M* ratio (5) of the three, has a crystal structure based on slabs of SiO_4 tetrahedra [lemoynite-type, $(Si_5O_{13})^{-6}$] joined by isolated TiO_6 octahedra. Thus, a progression from low to high *T*:*M* ratios in moving from labuntsovite-Mn → haineaultite → hogarthite is reflected in the crystal structures of these titanosilicate minerals, this involving an increase in polymerization of the silicate component and a concomitant decrease in the same for the titanate component. The impact of changes in the *T*:*M* ratios and the crystal structures on the paragenesis of hogarthite is discussed later.

As there are both Ti- and Zr-dominant members within the lemoynite group, the question arises as to whether Nb-dominant members of the group might also exist. Isomorphous substitution involving Ti and Zr is well-established (*cf.* Chakhmouradian & Williams 2004), this being strongly influenced by their crystal-chemical similarity [$^{[6]}Ti^{4+}$ = 0.61 Å, $^{[6]}Zr^{4+}$ = 0.72 Å; Shannon 1976]. The situation with Nb is slightly different, primarily with respect to charge [$^{[6]}Nb^{5+}$ = 0.64 Å; Shannon 1976], although isomorphous substitution between Ti^{4+} and Nb^{5+} in minerals is well-known (*e.g.*, the labuntsovite group;

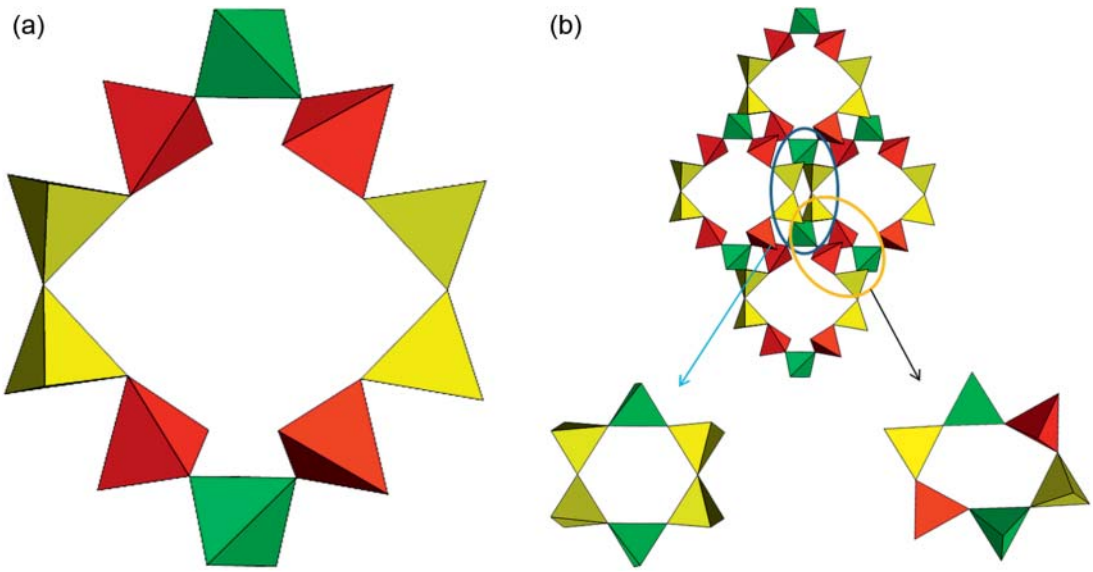

FIG. 6. (a) 10-membered silicate ring in hogarthite viewed along [102] with $Si(1)O_4$ tetrahedra in red, $Si(2)O_4$ in yellow, and $Si(3)O_4$ tetrahedra in green, and (b) linkages between adjacent 10-membered rings that lead to channels along [101] and the development of two different, additional six-membered rings (shown in insets).

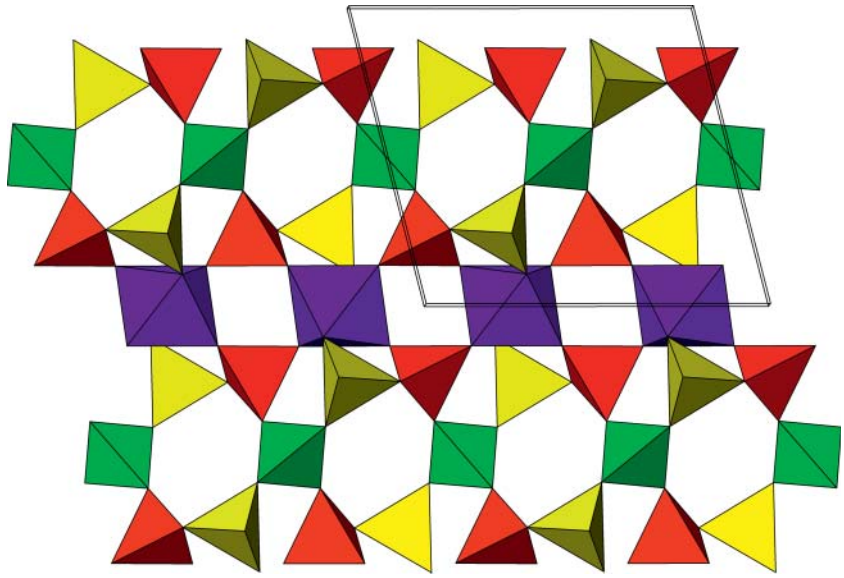

FIG. 7. The crystal structure of hogarthite viewed along [010] showing thick silicate layers separated by a layer of independent TiO_6 octahedra. One of the six-membered silicate rings is shown. The polyhedra shown are colored as in Figure 6 and the unit cell is shown.

Chukanov & Pekov 2005). It is also noteworthy that while $M O_6$ octahedra with Ti^{4+} and Nb^{5+} are easily polymerized, those with Zr^{4+} are not; in fact, the only known Zr-dominant MHM are those containing ZrO_6 octahedra isolated from one another, the explanation for which remains unclear. However, the isomorphous substitution of $Ti^{4+} \leftrightarrow Zr^{4+}$ in lemoynite-group minerals is consistent with this observation, given that they contain isolated $M O_6$ octahedra. The fact that no Nb-dominant members of the group have been found to date may simply be explained by the paucity of Nb^{5+} in those environments having $T{:}M > 3$. It is also conceivable, however, that subtle features relating to the coordination of Nb^{5+} may also play a role, these being that Nb^{5+} frequently occurs in both five- and six-coordinations (Piilonen *et al.* 2006), along with the fact that when in [6], the NbO_6 octahedron typically shows strongly anisotropic Nb–O bonds, principally along the axial directions (*e.g.*, 2.5 *versus* 1.8 Å in laurentianite; Haring *et al.* 2012). Both of these crystal-chemical features would necessarily impact on the linkages involving the $[MT_5O_{13}]$ unit, which serves as the fundamental building block in all lemoynite-group minerals. Such features could inhibit or place limitations on the extent to which complete $Zr^{4+} \leftrightarrow Ti^{4+} \leftrightarrow Nb^{5+}$ isomorphous substitution may occur. Regardless, the possibility of there being a Nb-dominant member of the lemoynite group must be considered high.

ORIGIN, PARAGENESIS, AND GENETIC IMPLICATIONS

The marble xenoliths found at Mont Saint-Hilaire (MSH) are now considered to be Paleozoic rather than Precambrian in age (Mandarino & Anderson 1989), based on the evidence (*e.g.*, the presence of Silurian- to Devonian-aged fossils) presented by McDonald & Chao (2004). Supporting evidence comes from Feininger & Goodacre (1995), who argue on the basis of gravity anomalies and field relations that the western Monteregians (including MSH) were derived from magmas that spread laterally along a Precambrian-Paleozoic unconformity and then rose into the overlying sediments of the Saint Lawrence Lowlands. The MSH intrusion is thus considered to be a laccolith at depth with a base more than 1 km above the unconformity. The transport of large Precambrian xenoliths up to these levels would therefore seem unlikely. Finally, data from stable-isotope analyses (C^{13}, O^{18}) of calcite in a marble xenolith from the Poudrette quarry overlap with those of limestone from the St. Lawrence Lowlands (Schilling *et al.* 2011). Thus, all these lines of evidence unequivocally indicate a Paleozoic origin for the marble xenoliths at MSH.

As described above, the two-phase, vuggy marble xenolith in which hogarthite was discovered appears to be different from those normally found at MSH.

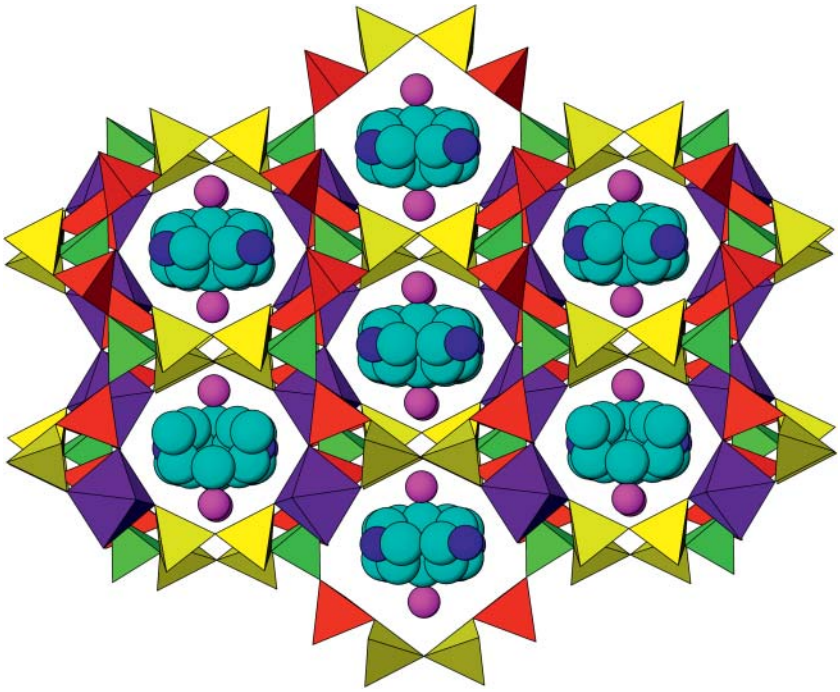

FIG. 8. The crystal structure of hogarthite viewed along [102] showing the channel occupants within the 10-membered rings. Sodium atoms are shown as pink spheres, Ca as dark blue spheres, and H_2O molecules as light blue spheres, with polyhedra colored as in Figure 6.

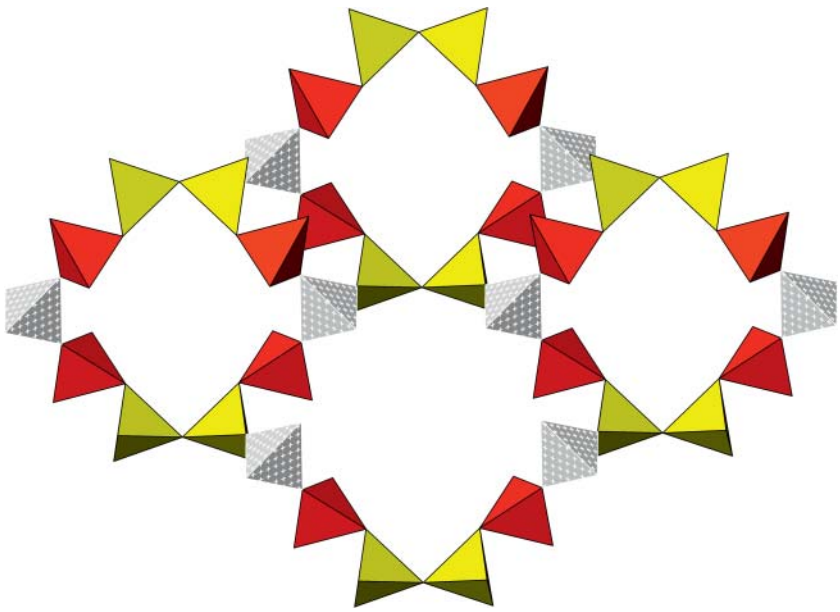

FIG. 9. The crystal structure of hogarthite showing the chains of silica tetrahedra with a periodicity of four. The $Si(1)O_4$ tetrahedra are shown in red and the $Si(2)O_4$ tetrahedra in yellow. The $Si(3)O_4$ tetrahedra, which link the chains, are grayed-out. The non-planar, interconnected 10-membered rings can be seen. Viewed along [102].

TABLE 8. BOND-VALENCE[1] TABLE (*v.u.*) FOR HOGARTHITE

	Na	*Ca**	*Ti*	*Si* 1	*Si* 2	*Si* 3	SUM
O1	$0.04^{x2\downarrow}$			0.95	1.00		1.99
O2					1.04	$1.06^{x2\downarrow}$	2.10
O3				1.00		$1.07^{x2\downarrow}$	2.07
O4					$1.07^{x2\rightarrow}$		2.14
O5		$0.23^{x2\downarrow}$	$0.69^{x2\downarrow}$	1.05			1.97
O6	$0.04^{x2\downarrow}$		$0.71^{x2\downarrow}$	1.05			1.80
O7		$0.34^{x2\downarrow}$	$0.66^{x2\downarrow}$		1.05		2.05
OW8*	$0.27^{x2\downarrow}$	$0.24^{x2\downarrow}$					0.39
OW9*		$0.28^{x2\downarrow}$					0.07
OW10*		0.27					0.07
OW11*							0.00
OW12*	0.17						0.17
SUM	0.38	1.68	4.12	4.05	4.16	4.26	

[1]Calculated using parameters from Brese & O'Keeffe (1991).
*Calculated using the SOF given in Table 6.

Most marble xenoliths are pale white to pale green in color, medium-grained, and composed of calcite with clinoamphibole. If vugs are present, the dominant minerals are pectolite, apophyllite-group minerals, mica-group minerals (phlogopite, tainiolite), vesuvianite, calcite, and Na-rich clinoamphiboles. Whereas the pale-colored portions of the hogarthite-bearing marble xenolith have attributes of the typical marble xenolith, the dark-colored portions and the vugs differ markedly in terms of texture (possible dissolution at contacts), color (general darkening to an almost black color), and in particular, mineralogy (*e.g.*, the presence of HFSE-bearing minerals). The metasomatic origin is supported not only by the presence of minerals rich in incompatible elements, but also by the observation that the contacts between the light- and dark-colored zones in the xenoliths are both irregular and diffuse, suggesting partial dissolution and possible replacement. The dark portions are thus interpreted to represent a metasomatized selvage, this being limited to <5 cm in thickness, produced through the interaction of a typical calcite-rich marble xenolith with a late-stage, incompatible-rich fluid. The fact that this metasomatized marble xenolith was noted to occur in a zone of brecciation is important, as it would represent a focused conduit along which

TABLE 9. COMPARATIVE DATA FOR LEMOYNITE-GROUP MINERALS

	Hogarthite	Natrolemoynite[1]	Altisite[2]	Lemoynite[3]
Chemical Formula	$(Na,K)_2CaTi_2Si_{10}O_{26}\cdot 8H_2O$	$Na_4Zr_2Si_{10}O_{26}\cdot 9H_2O$	$Na_3K_6Ti_2Al_2Si_8O_{26}Cl_3$	$(Na,K)_2CaZr_2Si_{10}O_{26}\cdot 5–6H_2O$
Space Group	*C*2/*m*	*C*2/*m*	*C*2/*m*	*C*2/*c*
Unit-Cell				
a	10.1839 (5)	10.5150 (2)	10.363 (2)	10.384 (3)
b	15.8244 (6)	16.2534 (4)	16.310 (3)	15.947 (7)
c (Å)	9.1327 (7)	9.1029 (3)	9.132 (2)	18.601 (6)
β (°)	104.463 (2)	105.462 (2)	105.34 (3)	104.59 (3)
V (Å^3)	1425.1 (1)	1499.4 (1)	1488.7 (4)	2980.9 (1)
Z	2	4	2	4
Strongest XRD Lines: (*I, d, hkl*)	80, 8.835, (001)	30, 8.832, (001)	71, 8.22, (020)	30, 8.832, (001)
	100, 7.913, (020)	100, 8.135, (020)	42, 3.50, (221)	100, 8.132, (020)
	70, 6.849, ($\bar{1}$11)	40, 5.975, (021)	35, 3.157, (240)	40, 5.975, (021)
	45, 4.336, ($\bar{1}$31,$\bar{1}$12)	35, 3.974, (201)	100, 3.049, (132)	35, 3.974, (201)
	80, 3.514, (221)	40, 3.564, (221)	71, 2.900, ($\bar{3}$31)	40, 3.564, (221)
	55, 3.426, ($\bar{2}$22,$\bar{1}$32)	35, 3.490, ($\bar{2}$22)	84, 2.835, (151)	35, 3.490, ($\bar{2}$22)

[1]McDonald & Chao 2001; [2]Khomyakov *et al.* 1995; [3]Perrault *et al.* 1969.

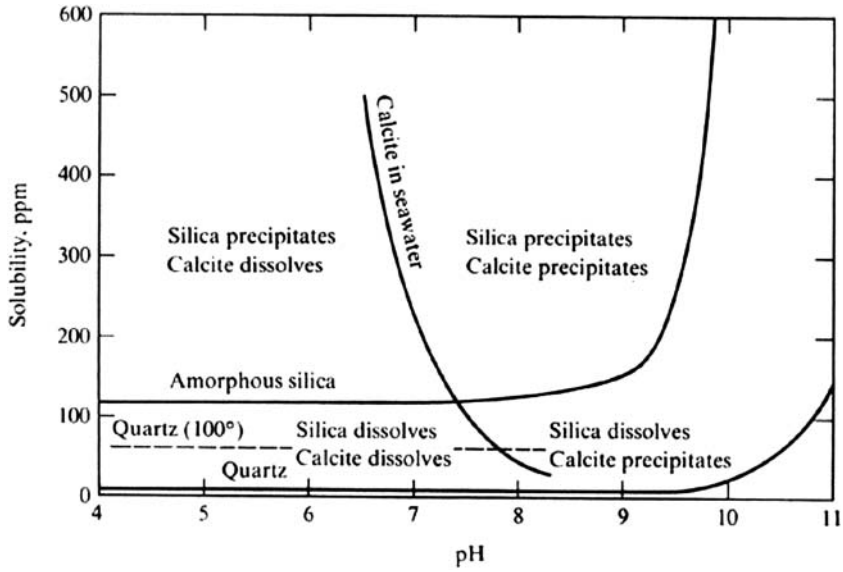

FIG. 10. The solubility of calcite and quartz as a function of pH and T (from Blatt *et al.* 1980).

late-stage, volatile- and incompatible-rich fluids, possibly originating from a crystallizing melt, would have preferentially moved. The breccia zone would thus have provided an enhanced opportunity for the interaction between pre-existing marble xenoliths and these late-stage fluids, leading to the metasomatism of the former.

The fluids responsible for the metasomatism would have been enriched in highly incompatible elements, including HFSE, REE, and LILE (including alkalis and alkaline-earths), along with water and volatiles. Such a geochemical suite would be expected to give rise to a mineral assemblage consistent with such enrichments, which is the case: along with pectolite, a mineral common in agpaitic environments, the metasomatized selvage also contains hogarthite and a götzenite-like mineral [ideally, $Na_2Ca_5Ti(Si_2O_7)_2F_4$], the latter being stabilized by conditions of high aF_2 and moderately high $aSiO_2$ (Andersen *et al.* 2012). The presence of yellow, possibly LREE-enriched, calcite in the vugs, bastnaesite-(Ce), and HFSE-enriched minerals (*e.g.*, tumchaite) also suggests the existence of an incompatible-rich, metasomatic fluid. The link between F-rich fluids and the development of HFSE-enriched minerals has been recently discussed by Demartis *et al.* (2014). These authors argue that a high F-content is important for transportation of LILE and HFSE in some LCT-type pegmatites and that crystallization of F-rich micas is key to the precipitation of HFSE-bearing minerals. This is an important concept, given the abundance of fluorite, along with the presence of F-enriched phlogopite, in the assemblage associated with hogarthite.

The vugs in the metasomatic selvage are lined by an early generation of coarse-grained, colorless, euhedral calcite (calcite-I) that is sometimes overgrown by a yellow to yellowish-orange calcite (calcite-II). In rare cases, the calcite-II can be overgrown by a subsequent generation of colorless calcite (calcite-III). The presence of the calcite-II is noteworthy, as it has a Raman spectrum (this study) that shows anomalous peaks in the region 1800–2500 cm^{-1} that may be due to fluorescence arising from an enriched LREE content, a feature previously noted in similar material associated with haineaultite (McDonald, unpublished data). Furthermore, calcite-II is commonly observed to strongly fluoresce pink to reddish-pink under medium-wave UV, whereas neither the calcite-I nor calcite-III does. Pink fluorescence is common in calcite, with Mn being considered the activator, but this effect is generally only observed under long-wave UV (Fonda 1940). At least two generations of quartz are present: (1) coarse-grained quartz (quartz-I), developing as crystals up to a few mm in length, and (2) drusy quartz (quartz-II), composed of euhedral crystals <1 mm in length. The drusy quartz overgrows both the calcite-II and quartz-I and is noteworthy in that it may, in some cases, exhibit a strong, green fluorescence under short-wave UV. As both calcite and quartz dominate the vugs, it is relevant to consider the conditions leading to their formation. The crystallization of calcite is sensitive to both T and pH, this occurring under conditions of relatively low T (*i.e.*, ~110 ºC) and high pH (>8), with SiO_2 being soluble under the same conditions (Fig. 10). As the vugs paragenetically show calcite overgrown by

quartz, this suggests initial formation of calcite under relatively high pH (>8) and low T (~110 ºC), possibly followed by the input of a secondary fluid of higher T, pH, or both, leading to the formation of quartz.

Three different titanosilicate minerals are observed in the vugs: labuntsovite-Mn, haineaultite, and hogarthite. Labuntsovite-Mn is the only one observed as inclusions in calcite-II, suggesting it is paragenetically earlier than either hogarthite or haineaultite. Both of the latter are overgrown by quartz-II, indicating they are paragenetically earlier, but the nature of the true relationship between the two titanosilicate minerals is not clear. The presence of quartz in the vugs of the marble xenoliths indicates a high $a\mathrm{SiO_2}$ and this, along with the relative Si:Ti ratios for haineaultite and hogarthite, suggests that the paragenesis is haineaultite → hogarthite. Taken together, a plausible paragenetic sequence involving the titanosilicate minerals found in the vugs is: labuntsovite-Mn → haineaultite → hogarthite. This reflects both an increase in $a\mathrm{SiO_2}$ and a concomitant decrease in $a\mathrm{TiO_2}$ with time. Finally, lemoynite, a Zr-dominant mineral, has also been observed in two vugs, in one case as fine, hair-like acicular crystals overgrowing hogarthite. This overgrowth relationship implies that the late-stage fluids were chemically evolving in the direction of Ti → Zr with time.

Recently, attention has been given to mesoporous zirconosilicates and their analogues, owing to their zeolitic-like properties. In particular, considerable effort has been made in synthesizing these phases, an important aspect of which is that these studies can provide data useful in constraining the conditions of formation relating to their mineralogical equivalents. For example, lemoynite can be synthesized from gels formed by combining $\mathrm{SiO_2}$, $\mathrm{ZrCl_4}$, NaOH, and distilled water, then heated to 200 ºC for 120 h (Petrova *et al.* 2011). These workers also showed through combined heating (TG-DTA) and powder X-ray diffraction analyses that lemoynite crystallizes at $T <$ 200 ºC with $C2/c$ space-group symmetry, but heating to >300 ºC results in a gradual loss of $\mathrm{H_2O}$, a relaxation of the crystal structure, and a change in the space-group symmetry to *Pbnm*, but with the original crystal-structure topology being retained. This crystal structure is stable up to $T < 1000$ ºC, beyond which it transforms irreversibly to a triclinic structure with space-group symmetry $P\bar{1}$, along with a concomitant structural modification and increase in density. In light of this information, along with the crystal-chemical and geochemical similarity of Zr and Ti, and the conditions under which the inorganic microporous titanosilicates ETS-4 and ETS-10 (which have crystal structures related to haineaultite; McDonald & Chao 2004) have been synthesized, hogarthite probably crystallized at low P at $T < 200$ ºC, from an alkaline fluid enriched in $\mathrm{SiO_2}$ and $\mathrm{TiO_2}$ (possibly through crystallization of a gel) and was not subsequently exposed to $T > 300$ ºC.

Acknowledgements

Our thanks go to M.A. Cooper and F.C. Hawthorne (Dept. of Geological Sciences, University of Manitoba) for providing access to, and assistance with, the four-circle diffractometer. We appreciate the assistance of Associate Editor A. Ertl and the comments of S. Mills. Financial support for the research was provided through a grant to AMM from the Natural Sciences and Engineering Research Council of Canada.

References

Andersen, T., Elburg, M., & Erambert, M. (2012) Petrology of combeite- and götzenite-bearing nephelinite at Nyiragongo, Virunga Volcanic Province in the East African Rift. *Lithos* **152**, 105–121.

Brese, N.E. & O'Keeffe, M. (1991) Bond-valence parameters for solids. *Acta Crystallographica* **B47**, 192–197.

Blatt, H., Middleton, G.V., & Murray, R.C. (1980) *Origin of Sedimentary Rocks.* Prentice Hall, Englewood Cliffs, New Jersey, United States, 634 pp.

Cannillo, E., Mazzi, F., & Rossi, G. (1966) The Crystal Structure of Neptunite. *Acta Crystallographica* **21**, 200–208.

Celestian, A.J., Powers, M., & Rader, S. (2013) In situ Raman spectroscopic study of transient polyhedral distortions during cesium ion exchange into sitinakite. *American Mineralogist* **98**, 1153–1161.

Chakhmouradian, A.R. & Williams, C.T. (2004) Mineralogy of high-field-strength element (Ti, Nb, Zr, Ta, Hf) in phosphoritic and carbonatitic rocks of the Kola Peninsula, Russia. *In* Phoscorites and carbonatites from Mantle to Mine: the Key Example of the Kola Alkaline Province (F. Wall & A.N. Zaitsev, eds.). *Mineralogical Society Series* **10**, 293–340.

Chukanov, N.V. & Pekov, I.V. (2005) Heterosilicates with Tetrahedral-Octahedral Frameworks: Mineralogical and Crystal-chemical Aspects. *In* Micro- and Mesoporous Mineral Phases (G. Ferraris & S. Merlino, eds.). *Reviews in Mineralogy and Geochemistry* **57**, 105–144.

Cromer, D.T. & Liberman, D. (1970) Relativistic calculation of anomalous scattering factors for X-rays. *Journal of Chemical Physics* **53**, 1891–1898.

Cromer, D.T. & Mann, J.B. (1968) X-ray scattering factors computed from numerical Hartree-Fock wave functions. *Acta Crystallographica* **A24**, 321–324.

Demartis, M., Melgarejo, J.C., Colombo, F., Alfonso, P., Coniglio, J.E., Pinotti, L.P., & D'Eramo, F.J. (2014)

Extreme F activities in late pegmatitic events as a key factor for LILE and HFSE enrichment: The Ángel pegmatite, central Argentina. *Canadian Mineralogist* **52**, 247–269.

Dowty, E. (2002) *CRYSCON for Windows and Macintosh, Version 1.1.* Shape Software Kingsport, Tennessee, USA.

Farmer, V.C. (1974) The infrared spectra of minerals. *Mineralogical Society Series*, London, United Kingdom, 539 pp.

Feininger, T. & Goodacre, A.K. (1995) The eight classical Monteregian hills at depth and the mechanism of their intrusion. *Canadian Journal of Earth Sciences* **32**, 1350–1364.

Fonda, G.R. (1940) The preparation of fluorescent calcite. *Journal of Physical Chemistry* **44**, 435–439.

Grice, J.D. & Gault, R.A. (2006) Johnsenite-(Ce), a New Member of the Eudialyte Group from Mount Saint Hilaire, Quebec, Canada. *Canadian Mineralogist* **44**, 105–116.

Haring, M.M., McDonald, A.M., Cooper, M.A., & Poirier, G.A. (2012) Laurentianite, $[NbO(H_2O)]_3(Si_2O_7)_2[Na(H_2O)_2]_3$, a new mineral from Mont Saint-Hilaire, Quebec: Description, crystal-structure determination and paragenesis. *Canadian Mineralogist* **50**, 1265–1280.

Khomyakov, A.P., Nechelyustov, G.N., Ferraris, G., & Ivaldi, G. (1995) Altisite, $Na_3K_6Ti_2Al_2Si_8O_{26}Cl_3$, a new mineral. *Zapiski Vserossiiskogo Mineralogicheskogo Obshchestva* **123(6)**, 90–95.

Liebau, F. (1985) *Structural chemistry of silicates.* Springer-Verlag, Berlin, Germany, 347 pp.

Mandarino, J.A. (1981) The Gladstone–Dale relationship. IV. The compatibility concept and its application. *Canadian Mineralogist* **19**, 441–450.

Mandarino, J.A. & Anderson, V. (1989) *Monteregian Treasures: The Minerals of Mont Saint-Hilaire, Quebec.* Cambridge University Press, Cambridge, England, 302 pp.

Mcardle, P., Gilligan, K., Cunningham, D., Dark, R., & Mahon, M. (2004) OSCAIL. *Crystal Engineering Communications* **6**, 303–309.

McDonald, A.M. & Chao, G.Y. (2001) Natrolemoynite, a new hydrated sodium zirconosilicate from Mont Saint-Hilaire, Quebec: Description and structure determination. *Canadian Mineralogist* **39**, 1295–1306.

McDonald, A.M. & Chao, G.Y. (2004) Haineaultite, a new hydrated sodium calcium titanosilicate from Mont Saint-Hilaire, Quebec: Description, structure determination and genetic implications. *Canadian Mineralogist* **42**, 769–780.

Petrus, J.A., Ross, K.C., & McDonald, A.M. (2012) DIIS: a cross-platform program for the reduction of X-ray diffraction data from a cylindrical area detector. *Computers & Geosciences* **38**, 156–163.

Petrova, N.R., Noriaki, N., Snejana, B., Petr, B., & Vladislav, K.-K. (2011) Temperature-induced phase transformations of the small-pore zirconosilicate $Na_2Zr_2Si_2O_7{\cdot}H_2O$. *Solid State Sciences* **13**, 1187–1190.

Perralut, G., Semenov, E.I., Bikova, A.V., & Capitonova, T.A. (1969) La lemoynite, un nouveau silicate hydrate de Zirconium et de sodium de St. Hilaire, Québec. *Canadian Mineralogist* **9**, 585–596.

Piilonen, P.C., McDonald, A.M., & Lalonde, A.E. (1998) The crystal chemistry of aegirine from Mont Saint-Hilaire, Quebec. *Canadian Mineralogist* **36**, 779–791.

Piilonen, P.C., McDonald, A.M., & Lalonde, A.E. (2003) Insights into astrophyllite-group minerals I: Nomenclature, composition and development of a standardized general formula. *Canadian Mineralogist* **42**, 1–26.

Piilonen, P.C., Farges, F., Linnen, R.L., Brown, G.E., Jr., Pawlak, M., & Pratt, A. (2006) Structural environment of Nb^{5+} in dry and fluid-rich (H_2O, F) silicate glasses: a combined XANES and EXAFS study. *Canadian Mineralogist* **44**, 775–794.

Schilling, J., Marks, M.A.W., Wenzel, T., Vennemann, T., Horvath, L., Tarassoff, P., Jacob, D.E., & Markl, G. (2011) The magmatic to hydrothermal evolution of the intrusive Mont Saint-Hilaire complex: insights into the late-stage evolution of peralkaline rocks. *Journal of Petrology* **52**, 2147–2185.

Shannon, R.D. (1976) Revised effective ionic radii and systematic studies of interatomic distances in halides and chalcogenides. *Acta Crystallographica* **A32**, 751–767.

Sheldrick, G.M. (1997) *SHELXL-97: A computer program for the Refinement of Crystal Structures.* University of Göttingen, Göttingen, Germany.

Sheldrick, G.M. (2008a) *SADABS.* University of Göttingen, Göttingen, Germany.

Sokolova, E.V., Rastsvetaeva, R.K., Andrianov, V.I., Egorov-Tismenko, Y.K., & Men'Shikov, Y.P. (1989) The crystal structure of a new sodium titanosilicate. *Soviet Physics Doklady* **34**, 583–585.

Received October 22, 2014, revised manuscript accepted March 6, 2015.